Bull. Mater. Sci., Vol. 35, No. 6, November 2012, pp. 919–924. © Indian Academy of Sciences.

Magneto-dielectric effect in $Pb(Zr_{0.52}Ti_{0.48})O_3$ filled nanoporous $Ni_{0.5}Zn_{0.5}Fe_2O_4$ composite

SHILPI BANERJEE[†,‡], ANINDYA DATTA[#], ASIM BHAUMIK[‡] and DIPANKAR CHAKRAVORTY[†,*]

[†]MLS Professor's Unit, [‡]Department of Materials Science, Indian Association for the Cultivation of Science, Kolkata 700 032, India

[#]University School of Basic and Applied Science (USBAS), Guru Govind Singh Indraprastha University, New Delhi 110 078, India

MS received 28 March 2012

Abstract. **Nanoporous $Ni_{0.5}Zn_{0.5}Fe_2O_4$ particles of diameter, ~ 9·5 nm, were synthesized by citric acid assisted thermal decomposition in an autoclave. The BET surface area measured was 80 m^2 g^{-1} and the average pore diameter was 2·5 nm. By soaking the particles in a suitable precursor solution and then subjecting them to a heat treatment at 923 K for 3 h, $Pb(Zr_{0.52}Ti_{0.48})O_3$ was grown within the nanopores. X-ray and electron diffraction studies confirmed the presence of both these phases. The nanocomposites showed ferromagnetic behaviour over the temperature range 2–300 K. No ferroelectric hysteresis loop could be found which was consistent with the earlier theoretical prediction of loss of ferroelectricity below a critical thickness of 2·4 nm. Good magneto-dielectric response of the order of 7% at a magnetic field of 9 kOe was recorded for the present system. This is believed to arise due to a negative magnetostriction coefficient of $Ni_{0.5}Zn_{0.5}Fe_2O_4$ which exerted a compressive strain on $Pb(Zr_{0.52}Ti_{0.48})O_3$ thereby lowering the tetragonality in its crystal structure.**

Keywords. **Magneto dielectric effect; nanocomposites; $Pb(Zr_{0.52}Ti_{0.48})O_3$; $Ni_{0.5}Zn_{0.5}Fe_2O_4$.**

1. Introduction

Multiferroic materials exhibit both ferroelectric and ferromagnetic properties. They have constituted an active area of research because of enormous application possibilities, some of which are multiple state memory systems, magnetic field sensors and signal processing devices (Rya *et al* 2002; Corral-Flores *et al* 2006; Tan *et al* 2008). Single phase multiferroic materials are rare in nature. The only reported compounds are some bismuth and rare-earth manganates (Hill and Rabe 1999; Filippetti and Hill 2001; Seshadri and Hill 2001; Fiebig *et al* 2002; Strempher *et al* 2007). Recently, some strain-induced multiferroic single phase systems have been reported (Bhattacharya *et al* 2010; Hajra *et al* 2011). However, single phase multiferroic materials do not show a reasonable value of magneto-electric coupling coefficient to make them suitable for a device. Composite multiferroic systems involving magnetostrictive and piezoelectric phases have been investigated extensively in recent times to get around the above mentioned difficulty. Efforts have been concentrated on synthesizing composites with both the phases having nanoscale dimensions. This gives better connectivity and coupling of the strains generated in the phases under the influence of the external field—either electric or magnetic. Multilayers of ferrites and piezoelectric phases were fabricated which showed large values of magneto-electric (ME) coefficient (Rya *et al* 2002; Srinivasan *et al* 2003; Fiebig 2005). Nanostructures of $CoFe_2O_4$–$BaTiO_3$ with a core-shell configuration were grown by a chemical method and their magneto-electric properties were investigated (Corral-Flores *et al* 2006, 2010; Raidongia *et al* 2010). Epitaxial $Pb(Zr_{0.53}Ti_{0.47})O_3/CoFe_2O_4$ multilayers of 11 layer thickness were prepared on suitable substrates by a pulsed-laser deposition technique (Zhang *et al* 2010). It was shown that interfacial strain engineering in the ferroelectric/ferromagnetic layered structure could tune the magneto-electric coupling. Thin films comprising $CoFe_2O_4$ nanopillars in a $BiFeO_3$ matrix were grown on $SrTiO_3$ substrates with a good value of magneto-electric coefficient (Yan *et al* 2009). $Ni_{0.5}Zn_{0.5}Fe_{1.95}O_{4-\delta}/PbZr_{0.52}Ti_{0.48}O_3$ composites were prepared by conventional ceramic method for using them as ME sensors and transducers (Venkata Ramana *et al* 2010). Core-shell structures of $Pb(Zr,Ti)O_3/NiFe_2O_4$ were prepared which showed high ME coefficient for a wide range of d.c. bias magnetic fields (Islam *et al* 2008).

We have explored the possibility of making a nanoporous ferrite first and subsequently filling the pores by a ferroelectric phase, $Pb(Zr_{0.52}Ti_{0.48})O_3$. It was thought that such a strategy would lead to better connectivity and strain coupling between the two phases when magnetic field was applied to the system. Recently, several research groups have reported on the synthesis of nanoporous oxides e.g. TiO_2, $SrTiO_3$, $BaTiO_3$, ZrO_2 (Wang *et al* 2006; Liu *et al* 2007, Hou *et al*

*Author for correspondence (mlsdc@iacs.res.in)

2008, 2009; He *et al* 2009; Mitra *et al* 2010a). A soft templating approach has been taken to make these materials. We have used citric acid assisted thermal decomposition technique to prepare our nanoporous ferrite. The magneto-dielectric parameter obtained was reasonably high. The results are reported in this paper.

2. Experimental

The first step was to prepare nanoporous $Ni_{0.5}Zn_{0.5}Fe_2O_4$ nanoparticles. For this nitrate salts of iron, nickel and zinc, respectively in proper amounts and citric acid monohydrate (molar ratio of total nitrate salt : citric acid monohydrate = 1:1·4) were separately milled and then mixed together. The mixture was put in an autoclave and heated at 453 K for 24 h. The product obtained was washed with distilled water and then dried at 333 K for a few hours. The formation of nickel zinc ferrite was confirmed by taking X-ray diffraction pattern using a model Bruker D8 diffractometer with CuK_α radiation. The pore surface area was found from adsorption isotherms measured by a Quantachrome Surface Area Analyser Autosorb-1C at 77 K.

The second step in sample preparation was to make a precursor solution for lead zirconate titanate of composition, $Pb(Zr_{0.52}Ti_{0.48})O_3$. A solution was prepared containing 20 ml of 2-methoxyethanol and 0·6 ml acetic acid. To this solution 0·057 ml zirconium butoxide was added followed after 10 min by 0·428 ml titanium isopropoxide. The mixing was done under continuous stirring. A transparent solution was obtained. Another solution was made by mixing 20 ml of 2-methoxyethanol, a few drops of concentrated nitric acid and 1·252 g of lead acetate under constant stirring. The two above mentioned solutions were mixed and then stirred for 2 h. The resultant solution was then allowed to age for 12 h without stirring. To the latter was then added the nanoporous nickel zinc ferrite powder synthesized as described previously. The soaking was carried out for a week. The resultant powder was then collected by centrifuging in ELTEK Research Centrifuge TC4100D. The powder was washed with 2-methoxyethanol and then with water. It was dried at 333 K for 12 h and then calcined at 923 K for 3 h.

To confirm the phases present in the material, X-ray diffraction pattern was taken using model Bruker D8 using CuK_α radiation. The microstructure of the nanocomposite was studied by a JEOL 2010 Transmission Electron Microscope operated at 200 kV. Optical absorption of the sample as a function of wavelength was measured using Cary 5000 UV-Vis-NIR spectrophotometer over the range from 200 to 800 nm using colloidal suspension of particles dispersed in ethanol.

Magnetization of the sample was measured over the temperature range 2 to 300 K in a Quantum Design MPMS system. For measurement of magneto-dielectric parameter the powder was compacted in a die of 1 cm diameter by applying a load of 5 ton. Both the surfaces were electroded by silver paint supplied by M/Acheson Colloiden, The Netherlands. The pellet sample was placed between the pole pieces of an electromagnet supplied by M/Control Systems and Devices, Mumbai, India. The capacitance change as a function of applied magnetic field was measured using an Agilent E4890A precision LCR meter.

3. Results and discussion

Figure 1 is the X-ray diffractogram obtained for nickel zinc ferrite powder. The peaks in this figure have been identified with the corresponding (*hkl*) planes of the ferrite phase. From the X-ray line broadening of the largest intensity peak (311) we calculated the average particle diameter to be ∼ 9·5 nm using Scherrer's formula (Cullity 1978).

Figure 2(a) shows nitrogen adsorption and desorption curves obtained for the porous nickel zinc ferrite. The pore width distribution was calculated using the NLDFT method (Jagiello and Betz 2008). In figure 2(b) is shown the pore size distribution as obtained by this method. The BET surface area was found to be 80 $m^2\ g^{-1}$ and the average pore diameter, 2·5 nm.

Figure 3 gives X-ray diffractogram for the composite powder soaked with lead zirconate titanate precursor solution and subsequently heat treated at 923 K for 3 h. It can be seen that the most intense peak (110) for $Pb(Zr_{0.52}Ti_{0.48})O_3$ phase is present indicating that the nanopores were filled with the same. The other peaks did not show up because of the very small thickness of lead zirconate titanate (∼2·5 nm).

Figure 4(a) is the optical absorption spectra obtained from the nanocomposite powder. We have plotted the corresponding $(\alpha h\nu)^2$ vs $h\nu$ data in figure 4(b), where α is the absorption coefficient, h the Planck's constant and υ the frequency of optical radiation. The determination of bandgap from optical absorption coefficient for crystalline materials has been done earlier by using Tauc's equation (Tsunekawa *et al* 2000; Saha *et al* 2011). The nature of variation of $(\alpha h\nu)^2$ as a function of $h\nu$ in the present case indicates that direct transitions are involved here. From this figure we extract two

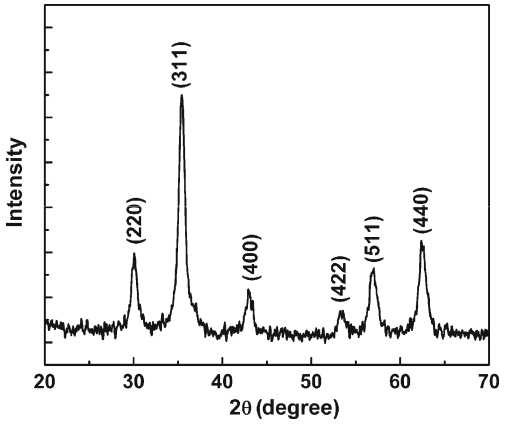

Figure 1. X-ray diffractogram of nanoporous nickel zinc ferrite powder synthesized by citric acid assisted thermal decomposition.

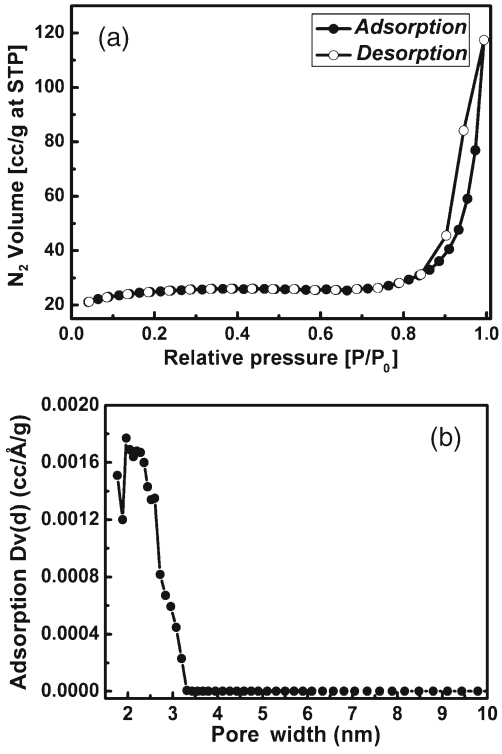

Figure 2. (**a**) N_2 adsorption/desorption isotherms of nanoporous nickel zinc ferrite powder and (**b**) NLDFT pore size distributions of nanoporous nickel zinc ferrite powder.

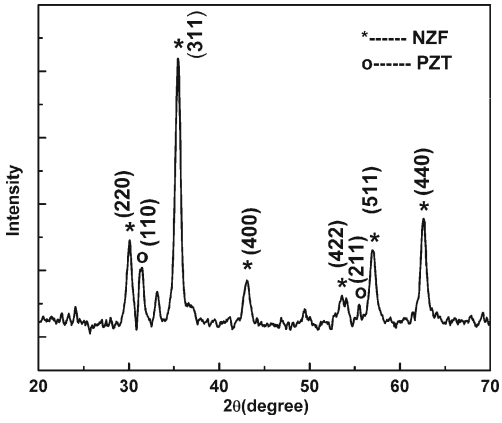

Figure 3. X-ray diffractogram of nanocomposite powder prepared by growing lead zirconate titanate phase in the pores of nanoporous nickel zinc ferrite.

band-gaps viz. 2·21 eV and 2·95 eV. These are believed to correspond to the phases of nickel zinc ferrite and lead zirconate titanate, respectively. Higher values than those of the bulk specimens arise due to quantum confinement effect.

Figure 5(a) is the transmission electron micrograph for the composite specimen. Cylindrical shaped particles can be seen. Fine strips of lead zirconate titanate phase can be seen as indicated by the arrows in the micrograph. Figure 5(b) is the electron diffraction pattern obtained from figure 5(a). The interplanar spacings were calculated from the positions of

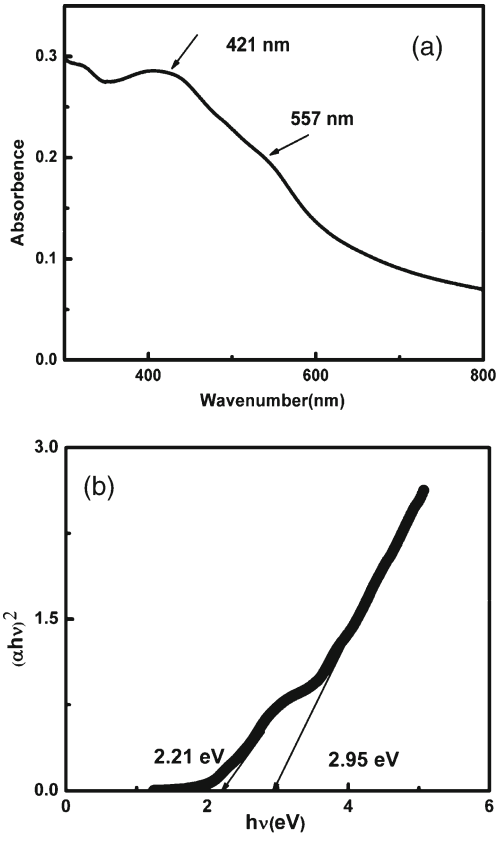

Figure 4. (**a**) UV–Vis absorption spectra of nanocomposite powder dispersed in ethanol in range 200–800 nm and (**b**) $(\alpha h\nu)^2$ vs $h\nu$ curve of nanocomposite powder.

the diffraction spots. The results are summarized in table 1. We have compared the d_{hkl} values as obtained from the X-ray and electron diffraction data with those of JCPDS file no. 08-0234 and 33-0784 values for $Ni_{0.5}Zn_{0.5}Fe_2O_4$ and $Pb(Zr_{0.52}Ti_{0.48})O_3$, respectively. It should be evident that both the phases are present in our nanocomposites. We also give the high resolution transmission electron micrograph in figure 5(c). The lattice images of some of the planes are indicated by arrows and their interplanar spacings are also shown. The presence of lead zirconate titanate phase within nickel zinc ferrite is evident. The two phases are shown by arrows in the image.

In figure 6 is shown the variation of magnetization as a function of temperature under both zero-field cooled (ZFC) and field cooled (FC) conditions. The nature of variation is the characteristic feature of superparamagnetic behaviour. Figure 7 gives the magnetization vs magnetic field curves at temperatures in the range 3–300 K. The inset shows a magnified view of the curves near low magnetic field. It is evident that the material exhibits ferromagnetic hysteresis loop even at room temperature. Figure 8 shows variation of coercive field, H_C, as obtained from figure 7 as a function of temperature. The coercivity decreases as the temperature is raised. This is expected in the case of an assembly of nanosized ferromagnetic particles. We have used the corresponding

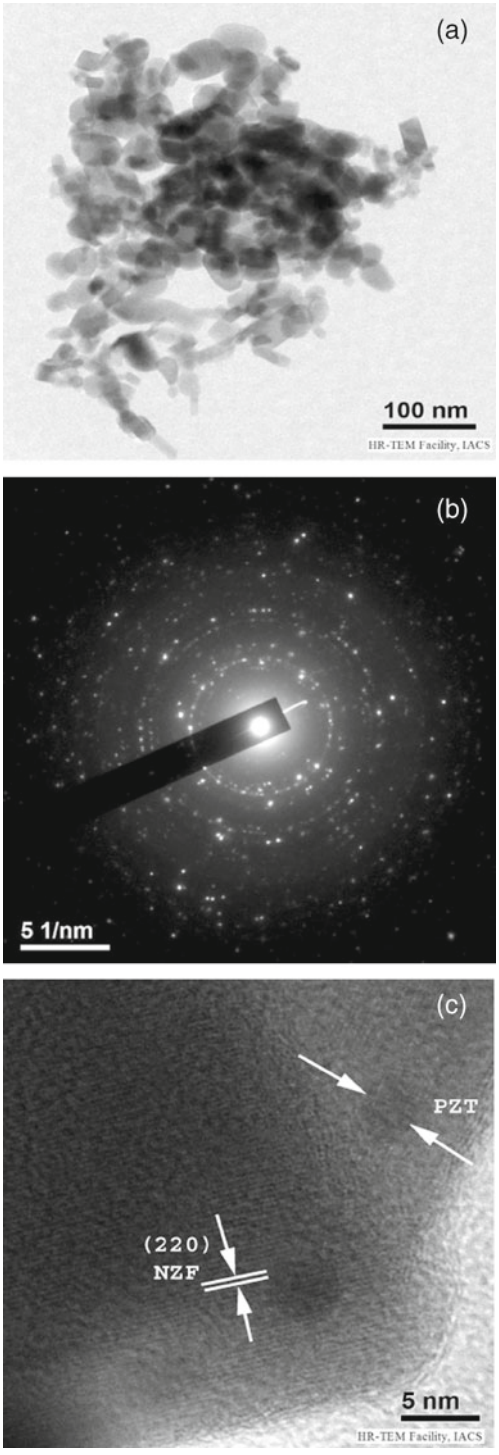

Figure 5. (**a**) Transmission electron micrograph showing morphology of nanocomposite powder, (**b**) electron diffraction pattern of figure 5(**a**) and (**c**) HRTEM image of nanocomposite powder.

relationship (Childress and Chien 1990) between H_C and T which is as follows

$$H_C = H_{CO}\left[1 - \left(\frac{T}{T_B}\right)^{1/2}\right], \quad (1)$$

Table 1. Comparison of d_{hkl} values obtained from electron diffraction rings from figure 5(b) with ASTM data.

Observed d_{hkl} (nm)	ASTM data of $Ni_{0.5}Zn_{0.5}Fe_2O_4$ (JCPDS no. 08-0234) (nm)	ASTM data of $Pb(Zr_{0.52}Ti_{0.48})O_3$ (JCPDS no. 33-0784) (nm)
0·308	0·2966(220)	
0·287		0·285(110)
0·256	0·2533(311)	
0·211	0·2110(400)	
0·149	0·1485(440)	

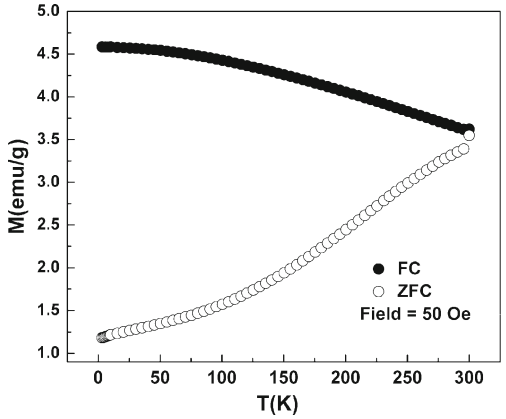

Figure 6. Magnetization vs temperature curve under ZFC and FC conditions at 50 Oe.

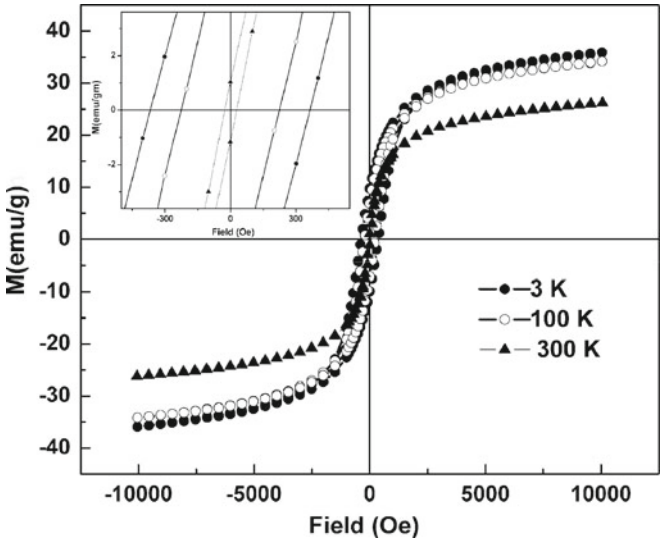

Figure 7. Magnetization vs magnetic field curve at different temperatures (3 K, 100 K and 300 K).

where $H_{C(0)}$ is the coercivity corresponding to 0 K, T the temperature and T_B the blocking temperature. The experimental data were fitted to (1) and the theoretical values are also shown in figure 8. There is a satisfactory agreement between the theoretical and experimental results. A value of $T_B = 361{\cdot}6$ K and $H_{CO} = 427{\cdot}5$ Oe were extracted from this fitting. This is consistent with the results shown in figure 6. Using the relation (Frei *et al* 1957)

$$T_B = \frac{KV}{25k_B}, \tag{2}$$

where K is the magnetocrystalline anisotropy, V the effective volume of the nanoparticle and k_B the Boltzmann constant. We have also calculated the value of K as $4{\cdot}0 \times 10^5$ erg/cc. It should be noted here that the robust ferromagnetic behaviour exhibited by the nanocomposite is contributed solely by the $Ni_{0.5}Zn_{0.5}Fe_2O_4$ phase. This has been verified by making detailed magnetic measurements on the latter without the presence of $Pb(Zr_{0.52}Ti_{0.48})O_3$ in it (Banerjee *et al* 2011, unpublished work).

Figure 9 gives variation of dielectric constant as a function of temperature for the nanocomposite specimen. We could not obtain good polarization-electric field hysteresis loops from our specimen. This is explained as arising due to ultrathin nature of $Pb(Zr_{0.52}Ti_{0.48})O_3$ grown within the nanopores of $Ni_{0.5}Zn_{0.5}Fe_2O_4$. As mentioned earlier the average pore diameter of $Ni_{0.5}Zn_{0.5}Fe_2O_4$ was found to be 2·5 nm and the $Pb(Zr_{0.52}Ti_{0.48})O_3$ phase was grown within this space. It has been reported before that ferroelectric material having a thickness <2·4 nm lose their ferroelectric properties (Junquera and Ghosez 2003; Dan *et al* 2005). It is, therefore, concluded that in our specimen system the ferroelectric phase has a thickness close to this threshold value. However, good magneto-dielectric response has been shown by the present nanocomposite system.

Figure 10 shows variation of $(\varepsilon(H)-\varepsilon(0))/\varepsilon(0)$ as a function of applied magnetic field, where $\varepsilon(H)$ and $\varepsilon(0)$ refer to the dielectric constants for magnetic fields, H and zero, respectively. It can be seen that the dielectric constant decreases as the magnetic field is increased. A decrease of almost 7% was recorded at an applied field of 9 kOe. We consider first the possibility of a magneto-resistance effect in the $Ni_{0.5}Zn_{0.5}Fe_2O_4$ phase. There is no report in the literature showing this property in the case of $Ni_{0.5}Zn_{0.5}Fe_2O_4$. Even if such an effect were present in our system, that would contribute to a lowering/increasing of resistance of the $Ni_{0.5}Zn_{0.5}Fe_2O_4$ phase. In the latter situation an inhomogeneous medium model (Parish and Littlewood 2008) could be invoked. We have tried to fit our data (dielectric constant vs magnetic field) to the above mentioned model as per our earlier work on a different system (Mitra *et al* 2010b) without success. In view of the above we explain the results as follows. When a magnetic field is applied to the material, the $Ni_{0.5}Zn_{0.5}Fe_2O_4$ phase shrinks because of a negative magnetostriction coefficient (Smit and Wijn 1959). This exerts a strain on the $Pb(Zr_{0.52}Ti_{0.48})O_3$ phase which is embedded within the $Ni_{0.5}Zn_{0.5}Fe_2O_4$ phase. The nature of strain is compressive in the present case. As a result the tetragonality is lowered and the off-centre positions of the Zr^{+4} and Ti^{+4} ions get shifted in such a way as to reduce the permanent dipole moment of the unit cell. This causes a lowering of the dielectric constant of the material.

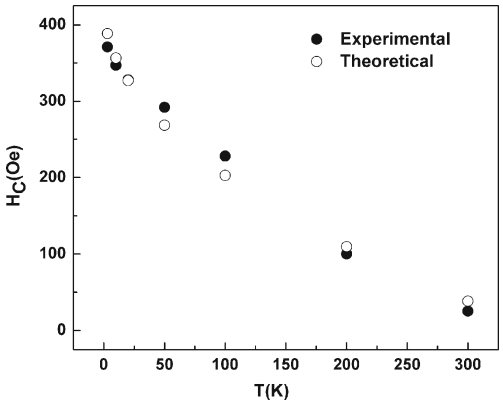

Figure 8. Variation of coercive field (extracted from M–H loops at different temperatures) as a function of temperature.

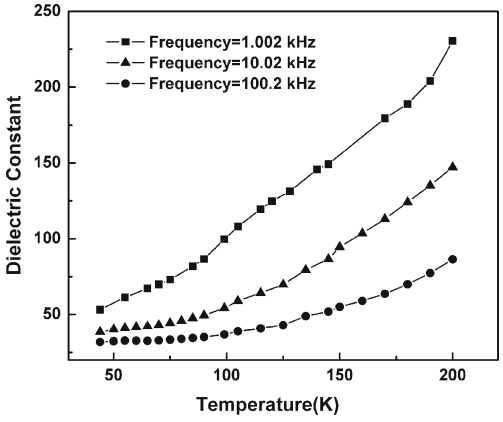

Figure 9. Variation of dielectric constant of nanocomposite at different frequencies as a function of temperature.

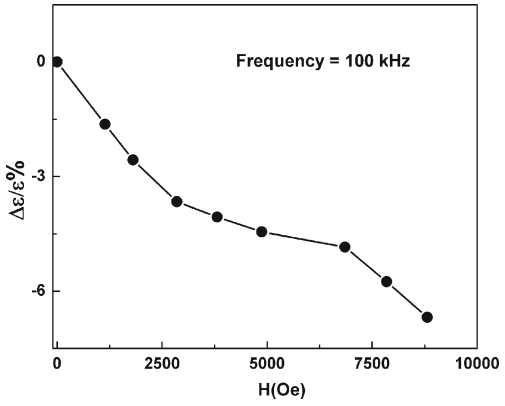

Figure 10. Variation of magneto-dielectric (MD) parameter as a function of applied magnetic field for nanocomposite powder.

4. Conclusions

In summary, we have synthesized nanoporous $Ni_{0.5}Zn_{0.5}Fe_2O_4$ particles of diameter 9·5 nm using citric acid assisted thermal decomposition in an autoclave. The BET surface area was 80 $m^2\ g^{-1}$ and the average pore diameter was 2·5 nm. These particles were soaked in a suitable precursor solution containing lead, zirconium and titanium, respectively. After suitable heat treatment, $Pb(Zr_{0·52}Ti_{0·48})O_3$ was found to grow within the nanopores as confirmed by X-ray diffraction and electron diffraction studies. The nanocomposite showed ferromagnetic behaviour over a temperature range 3–300 K. Magnetization studies under zero-field cooled and field cooled conditions showed a superparamagnetic behaviour. No ferroelectric hysteresis loop could be detected which was consistent with the theoretical prediction of loss of ferroelectricity below a critical thickness of 2·4 nm. However, good magneto-dielectric response of the order of 7% at a magnetic field of 9 kOe was recorded. This is explained as arising due to a negative magnetostriction coefficient of $Ni_{0.5}Zn_{0.5}Fe_2O_4$ which exerts a compressive strain on $Pb(Zr_{0·52}Ti_{0·48})O_3$ thus bringing about a lowering of tetragonality in its crystal structure.

Acknowledgements

This work was carried out under a project of DST Unit on Nanoscience supported by Department of Science and Technology, Govt. of India, New Delhi, under Nano Mission programme. One of the authors (SB) thanks the Council of Scientific and Industrial Research, New Delhi, for the award of a senior research fellowship. (DC) thanks the Indian National Science Academy, New Delhi, for the award of an honorary scientist's position.

References

Bhattacharya S, Datta A and Chakravorty D 2010 *Appl. Phys. Lett.* **96** 093109

Banerjee S, Datta A, Bhunia M K, Bhaumik A and Chakravorty D 2011 Unpublished

Childress J R and Chien C L 1990 *Appl. Phys. Lett.* **56** 95

Corral-Flores V, Bueno-Baques D, Carrillo-Flores D and Matutes-Aquino J A 2006 *J. Appl. Phys.* **99** 08J503

Corral-Flores V, Bueno-Baques D and Ziolo R F 2010 *Acta Mater.* **58** 764

Cullity B D 1978 *Elements of X-ray diffraction* (Boston: Addison Wesley) p. 99

Dan A, Mukherjee P K and Chakravorty D 2005 *J. Mater. Chem.* **15** 1477

Fiebig M 2005 *J. Phys. D: Appl. Phys.* **38** R123

Fiebig M, Lottermoser T, Frohlich D, Goltsev A V and Pisarev R V 2002 *Nature (London)* **419** 818

Filippetti A and Hill N A 2001 *J. Magn. Magn. Mater.* **236** 176

Frei E H, Shtrikman S and Treves D 1957 *Phys. Rev.* **106** 4

Hajra P, Dutta S, Brahma P and Chakravorty D 2011 *J. Magn. Magn. Mater.* **323** 864

He C, Tian B and Zhang J 2009 *Micropor. Mesopor. Mat.* **126** 50

Hill N A and Rabe K M 1999 *Phys. Rev.* **B59** 8759

Hou R Z, Ferreira P and Vilarinho P M 2008 *Micropor. Mesopor. Mat.* **110** 392

Hou R Z, Ferreira P and Vilarinho P M 2009 *Chem. Mater.* **21** 3536

Islam R A, Bedekar V, Poudyal N, Ping Liu J and Priya S 2008 *J. Appl. Phys.* **104** 104111

Jagiello J and Betz W 2008 *Micropor. Mesopor. Mater.* **108** 117

Junquera J and Ghosez P 2003 *Letters Nature* **422** 506

Liu S G, Wang H, Li J P, Zhao N, Wei W and Sun Y H 2007 *Mater. Res. Bull.* **42** 171

Mitra A, Vázquez-Vázquez C, López-Quintela M R, Paul B K and Bhaumik A 2010a *Micropor. Mesopor. Mater.* **131** 373

Mitra S, Mandal A, Datta A, Banerjee S and Chakravorty D 2010b *Eur. Phys. Lett.* **92** 26003

Parish M M and Littlewood P B 2008 *Phys. Rev. Lett.* **101** 166602

Raidongia K, Nag A, Sundaresan A and Rao C N R 2010 *Appl. Phys. Lett.* **97** 062904

Rya J, Priya S, Uchino K and Kim H E 2002 *J. Electroceram.* **8** 107

Saha D R, Datta A, Mandal S, Mukherjee M, Nandi A K and Chakravorty D 2011 *Solid State Ionics* **186** 14

Seshadri R and Hill N A 2001 *Chem. Mater.* **13** 2892

Smit J and Wijn H P J 1959 *Ferrites* (New York: John Wiley & Sons) p. 169

Srinivasan G, Rasmussen E T and Hayes R 2003 *Phys. Rev.* **B67** 014418

Strempher J *et al* 2007 *Phys. Rev.* **B75** 212402

Tan S Y, Shannigrahi S R, Tan S H and Tay F E H 2008 *J. Appl. Phys.* **103** 094105

Tsunekawa S, Fukuda T and Kasuya A 2000 *J. Appl. Phys.* **87** 1318

Venkata Ramana M, Ramamanohar Reddy N, Murty B S, Murthy V R K and Siva Kumar K V 2010 *Adv. Condens. Matter Phys.* doi: 10.1155/2010/763406

Wang Y, Xu H, Wang X, Zhang X, Fia H, Zhang L and Qiu J 2006 *J. Phys. Chem.* **B110** 13835

Yan L, Xing Z, Wang Z, Wang T, Lei G, Li J and Vichland D 2009 *Appl. Phys. Lett.* **94** 192902

Zhang J X, Dai J Y and Chan H L W 2010 *J. Appl. Phys.* **107** 104105